# Dynamic Discharge and Performance of a New Adsorbent for Natural Gas Storage

**S. Biloe and V. Goetz**
Rambla de la Thermodynamique, IMP-CNRS UPR 8521, Institut de Science et Génie des Matériaux et Procédés, 66100 Perpignan, France

**S. Mauran**
Université de Perpignan, 66860 Perpignan cedex, France

*Performance of a new highly conductive adsorbent matrix for ANG systems was evaluated. The adsorbent composite block (ACB) was a mixture of superactivated carbon, labeled MAXSORB and expanded natural graphite (ENG), followed by consolidation. ENG was used both as a very high conductive matrix and as support for adsorbents. Thermal conductivity is 30 times higher than that of activated carbon packed bed. Dynamic methane discharges were studied experimentally with a 2-L vessel filled with ACB. The influence of both the discharge flow rate and heat-exchange conditions at the reactor wall on the delivered methane capacity was investigated. The modeling of the discharge process, validated from experimental results, shows the efficiency of this ACB with a 100-V/V delivered methane capacity under various working conditions.*

## Introduction

Natural gas vehicles (NGVs) provide numerous benefits both as alternative fuel and as clean and safety fuel (Talu, 1992; Wegrzyn and Gurevich, 1996). Natural gas is made up of 90% methane. It is lighter than air and is only flammable with about 10% volume in air. In addition, its ignition temperature is close to 650°C, compared with 250°C for gasoline.

Due to its low-energy density per unit volume (Parkyns and Quinn, 1995), current NGVs employ compressed natural gas (CNG). There are more than one million NGVs worldwide today (De Chauveron, 1996). However, this technology requires high pressure (20 MPa). High economic cost coupled with a large mass of onboard reservoirs limit the practical use of CNG technology.

A promising solution involves the use of suitable microporous materials. An adsorbed natural-gas (ANG) system can store natural gas by adsorption under moderate pressure: 3.5 MPa (Wegrzyn and Gurevich, 1996). The key to the successful ANG storage is the development of highly microporous adsorbents, that is, activated carbon and zeolites. Natural-gas storage capacity of a suitable adsorbent is currently expressed in terms of the stored volume of natural gas per unit of adsorbent volume, measured at normal conditions ($P = 0.1$ MPa, $T = 273$ K). To be a commercially viable system, a delivered 150 V/V is necessary (Parkyns and Quinn, 1995).

Many researchers deal with the development of highly microporous adsorbents with high packing densities and large specific surface areas (Alcañiz-Monge et al., 1997; Baker, 1998; MacDonald and Quinn, 1996, 1998; Manzi et al., 1997; Schwarz et al., 1998), and simulations of the dynamic discharge of ANG vessel (Chang and Talu, 1996; Lamari et al., 2000; Mota et al., 1995, 1997a,b; Zhou, 1996). On the other hand, few studies have been carried out on the experimental results (Chang and Talu, 1996; Jasionowski et al., 1989).

Numerous aspects occur in ANG storage systems that affect its performance, and hence, its viability. First, when discharging an isothermal ANG vessel, an amount of gas is retained at depletion pressure. The isothermal delivery gas capacity is therefore reduced by 10–15% of the total stored gas capacity. Second, the thermal effects, relating to both heat adsorption and desorption, which are 12–16 $kJ \cdot mol^{-1}$ for methane adsorption on activated carbon (Loughlin et al., 1993; Parkyns and Quinn, 1995; Rychlicki and Terzyk, 1995; Salem et al., 1998), limit the stored and the delivered gas capacity, respectively. Therefore, a loss of 35%, compared to an isothermal charge, can occur when charging an ANG vessel under the adiabatic condition (Chang and Talu, 1996;

Correspondence concerning this article should be addressed to V. Goetz.

Mota et al., 1997a). Third, the rate of fill and discharge is a major factor influencing the exothermic and endothermic effects (Chang and Talu, 1996). Experimental results have shown that the stored gas capacity is reduced dramatically from 127 V/V to 76 V/V for an adiabatic fast fill (Jasionowski et al., 1989). The ideal way is to charge and discharge natural gas at a low enough flow rate to get closer to isothermal conditions. Nevertheless, if the charge can be performed over a long time (overnight for the buses fleets), the discharge flow rate is controlled by the energy demand of a natural gas motor vehicle. A discharge flow rate of a 25 $Nl \cdot min^{-1}$ corresponds to the energy demand of a car traveling at cruising speed (Chang and Talu, 1996). In addition, the required high packing densities of activated carbon beds could create mass-transfer problems that limit in the same way the delivered capacity when discharging an ANG vessel (Cook et al., 1999). Consequently, the performances of ANG systems closely depend on the heat- and mass-transfer properties of the adsorbent. The ANG system is sometimes unable to meet the energy demand in real working conditions (Chang and Talu, 1996). Facing these problems, it is more important to focus on the delivered volume of methane than stored volume in ANG technology.

Few solutions have been proposed and discussed in the literature to reduce the thermal effects generated during the filling and the discharge of natural-gas storage cylinders. The first approach consists of enhancing the thermal capacity by using an *in situ* phase-change material (salt hydrate) that consumes the heat of adsorption and supplies it during the discharge process (Jasionowski et al., 1989; Mota, 1995). However, this material must have a specific melting point near the ambient temperature, whereas ANG technology is supposed to operate under various ambient conditions. Moreover, this approach is limited by the disadvantage that the occupying place by the change phase material is about 18% of the total volume. The second solution, proposed by Chang and Talu (1996), is to enhance heat transfer from the wall to the center of the ANG vessel by inserting a perforated tube into the center of the vessel (gas diffuser). By changing the axial flow to radial flow, the temperature distribution in the vessel is more uniform and allows reduction of the dynamic loss. Furthermore, the place occupied by the perforated tube is only 2% of the total volume. The last solution consists of enhancing the conductivity of the adsorbent. Indeed, the poor conductivity of the currently activated carbon packed bed is not appropriate for their use in ANG technology, since the volume of the delivered gas at depletion pressure decreases as the activated carbon bed temperature decreases.

In this article, the enhancement of both conductive heat transfer and heat exchange from the ANG vessel to the sur-

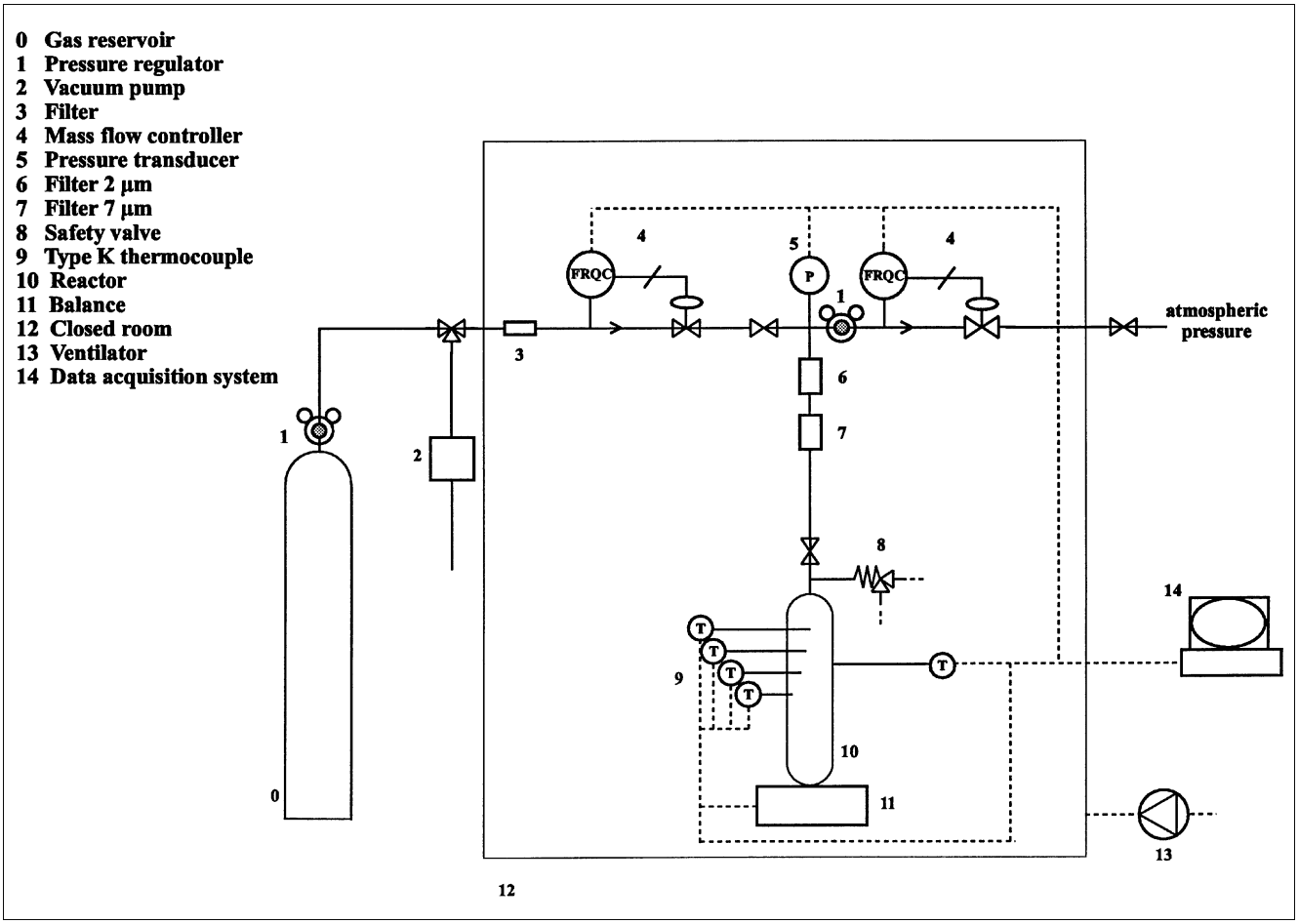


**Figure 1. Experimental laboratory device.**

roundings are investigated. The enhancement of the effective thermal conductivity, while keeping good mass-transfer properties, is performed by using a highly conductive matrix, made up of expanded natural graphite (ENG) and superactivated carbon (Maxsorb). On the other hand, to increase the flow of heat desorption from the vessel to the surroundings, the vessel wall is maintained externally at a fixed temperature by using an annular space wrapping around the vessel, where a fluid (water) can flow axially by forced convection.

ENG is produced by a rapid heating (1,000°C) of graphite intercalated compounds (GICs) obtained from natural graphite flakes (Ferrière et al., 2000; Yoshida and Hishiyama, 1991). Current GICs were prepared by chemical oxidation with $HNO_3$ in a concentric sulfuric acid. ENG is highly porous ($\epsilon > 0.8$) and has been used as a conductive medium and support for materials (salts) in thermochemical processes (Mauran et al., 1994). The Maxsorb activated carbon, which was referred to in the past as PX-21 (Amoco patent) and AX-21 (Anderson Development Company license) is now produced and sold under license by Kansai Coke and Chemicals Company Ltd. It presents a large microporous volume and a high surface area (Carrott et al., 2000; Kaneko and Murata, 1997; Otowa et al., 1993; Quirke and Tennison, 1996). It already has been used for the storage of methane (Jasionowski et al., 1989; Manzi et al., 1997).

The purpose of the present work is to investigate the behavior of ANG systems during discharge, with this new adsorbent composite block (ACB), made from Maxsorb and ENG. A model was developed to predict the performances of this new composite and to evaluate its benefits in terms of methane delivery amount per unit adsorbent volume, under real working conditions. The coupled heat- and mass-transfer model also has been developed in order to understand the phenomenon that could limit the performances. Experimental measurements are then compared with simulated results in order to validate the model presented.

## Experimental Study

### *Experimental laboratory apparatus*

Figure 1 shows the experimental laboratory device. A stainless-steel vessel of 2 mm thickness with a volume of about 2 L (diameter $\times$ length: 110.3 $\times$ 215 mm) was filled with the new ACB. Four thermocouples are distributed radially throughout the high-pressure vessel with a spacing of 1.1 cm, and one on the reactor wall to evaluate the thermal gradients during desorption. A classic pressure transducer and two mass flow controllers record and control the pressure and the gas flow, respectively. The amount of adsorbed gas at pressure charge ($P_c = 3.5$ MPa) was measured simultaneously by the mass flow controller and a gravimetric balance (Sartorius excellence, model E 12100S) of 12-kg capacity with a 0.1-g resolution. For safety reasons, a safety valve (calibrated at 4.0 MPa) was on top of the storage vessel, and the apparatus was placed in a safely-closed room. All the data were collected at the interface of a microcomputer. Finally, pure methane (99.99%) was used instead of natural gas in order to prevent reducing the stored capacity due to natural gas composition (Mota, 1999).

### *Experimental procedure*

The experimental procedure is described as follows:

- At the start of each run, the storage vessel was degassed during 14 h at a pressure of at least $10^2$ Pa.
- The data-acquisition system was activated.
- A constant volumetric flow rate of methane in the 1–10-$Nl \cdot m^{-1}$ range was introduced into the reservoir containing ACB. The adsorption step was terminated after the equilibrium was reached ($P_c = 3.5$ MPa, $T_o = 298.15$ K).
- During the desorption step, a constant volumetric flow rate of methane was applied via the downstream mass flow controller. The experimental procedure was terminated when the vessel was at uniform room temperature and depletion pressure ($P_o = 0.1$ MPa). The amounts of methane recovered by desorption down to atmospheric pressure and the temperatures were recorded as a function of time throughout the experimental procedure.

Different external heat-exchange conditions at the vessel wall were performed. The external fluid can be water as well as air. When water was the external fluid, the storage vessel was placed in a cylindrical reservoir (diameter $\times$ length = 150 $\times$ 400 mm) where water flows axially at constant temperature and flow rate. One run was performed with fiberglass insulation wrapped around the storage vessel, and a second one without a controlled discharge flow rate. The values of the wall–heat exchange coefficients were calculated in detail later. These different configurations assess the importance of the phenomenon that could limit the performances.

### *Adsorbent composite block*

ACBs were prepared by mixing ENG and activated carbon powder and then by consolidating directly in the ANG cylinder (diameter $\times$ height: 110.3 $\times$ 215 mm).

Maxsorb is a well-known high surface-area active carbon, but it has a low bulk density (Table 1). However, in onboard natural gas vehicles, the adsorbent must have a high bulk density, and should not be friable. ENG is a vermiculite material of a puffed-up appearance (Figure 2a) with a shape factor length/diameter of about 15 and a very low bulk density of 3 $kg \cdot m^{-3}$. It has a wide range of applications relating to both its thermal and mechanical properties (Lepinasse et al., 1994; Py et al., 2001; Toyoda and Inagaki, 2000; Union Carbide Trademark, 1968). However, the simple mixture of ENG with Maxsorb followed by compression does not produce a consolidated ACB. So the manufacturing procedure is based on the simultaneous use of a thermoplastic polymer [polyvinyl alcohol (PVA); polyethylene glycol PEG)] as a mechanical binder, already proposed and tested (Bose et al., 1990), and ENG as a thermal binder, with superactivated carbon powder. The experimental procedure has been previously reported (Biloé et al., 2001). It leads to a consolidated matrix (Figure 2b). The consolidation ensures the decrease of the intergranular porosity and should increase the contact between the Maxsorb powder and the ENG. In addition, the *in situ* compression in the reactor induces an anisotropic consolidated matrix with two main directions, parallel and orthogonal (also called radial), to the uniaxial direction of compression. The preferential orientation of graphite layers nor-

**Table 1. Technical Data for Maxsorb**

| | |
|---|---|
| BET surface area ($m^2 \cdot g^{-1}$) | 3,270 |
| Bulk density ($kg \cdot m^{-3}$) | 300 |
| Total pore volume for $r < 150$ Å ($m^3 \cdot kg^{-1}$) | $1.83 \times 10^{-3}$ |
| Moisture (%) | 0.5 |
| Ash (%) | 0.3 |
| pH | 3.7 |
| Mean particle diameter ($\mu$m) | 72 |

**Table 2. Transfer Properties and Adsorption Characteristics of the Adsorbent Composite Matrix**

| | |
|---|---|
| $\rho_s$ ($kg \cdot m^{-3}$) | 450 |
| $w_1$ (%) | 25 |
| $\epsilon_o$ | 0.81 |
| $k$ ($m^2$) | $1 \times 10^{-14}$ |
| $\lambda$($W \cdot m^{-1} \cdot K^{-1}$) | 7.3 |
| $W_o$ ($cm^3 \cdot g^{-1}$) | 1.17 |
| $E_o$ ($J \cdot mol^{-1}$) | 15,884 |
| $n$ | 1.39 |

mal to the direction of compression enhances the heat and mass transfer in the radial direction (Mauran et al., 1993). ACB was characterized by both its apparent density ($\rho_s$) and its weight ratio of ENG ($w_1$). In this article, the composite used for the experimental measurements has a weight ratio of 25% of ENG, and an apparent density of 450 $kg \cdot m^{-3}$ (Table 2).

## Model

In this article, the proposed model takes its inspiration from current models described elsewhere (Lamari et al., 2000; Mota et al., 1995, 1997a,b). The first objective of the model presented is to gauge the thermal behavior of the ANG vessel discharge and to evaluate the performance in terms of delivered methane capacity under various conditions.

### *The general assumptions*

The system is modeled on the form of three distinct media (Figure 3): the ACB, the external fluid, and the vessel wall separating them. Each of its media is subject to specific assumptions described as follows:

- The geometry ratio (diameter/length) of the reactor and the presence of a gas diffuser allow us to consider a one-dimensional problem according to the radial direction. All the axial effects are neglected.
- The reactive gas phase (methane) behaves as an ideal gas. The gas properties are thought to be constant in the range of temperature and pressure (1–3.5 MPa, 245–298 K). Mean values are taking into account. Also, the physical properties of both the tube and the external fluid (specific heat, density,

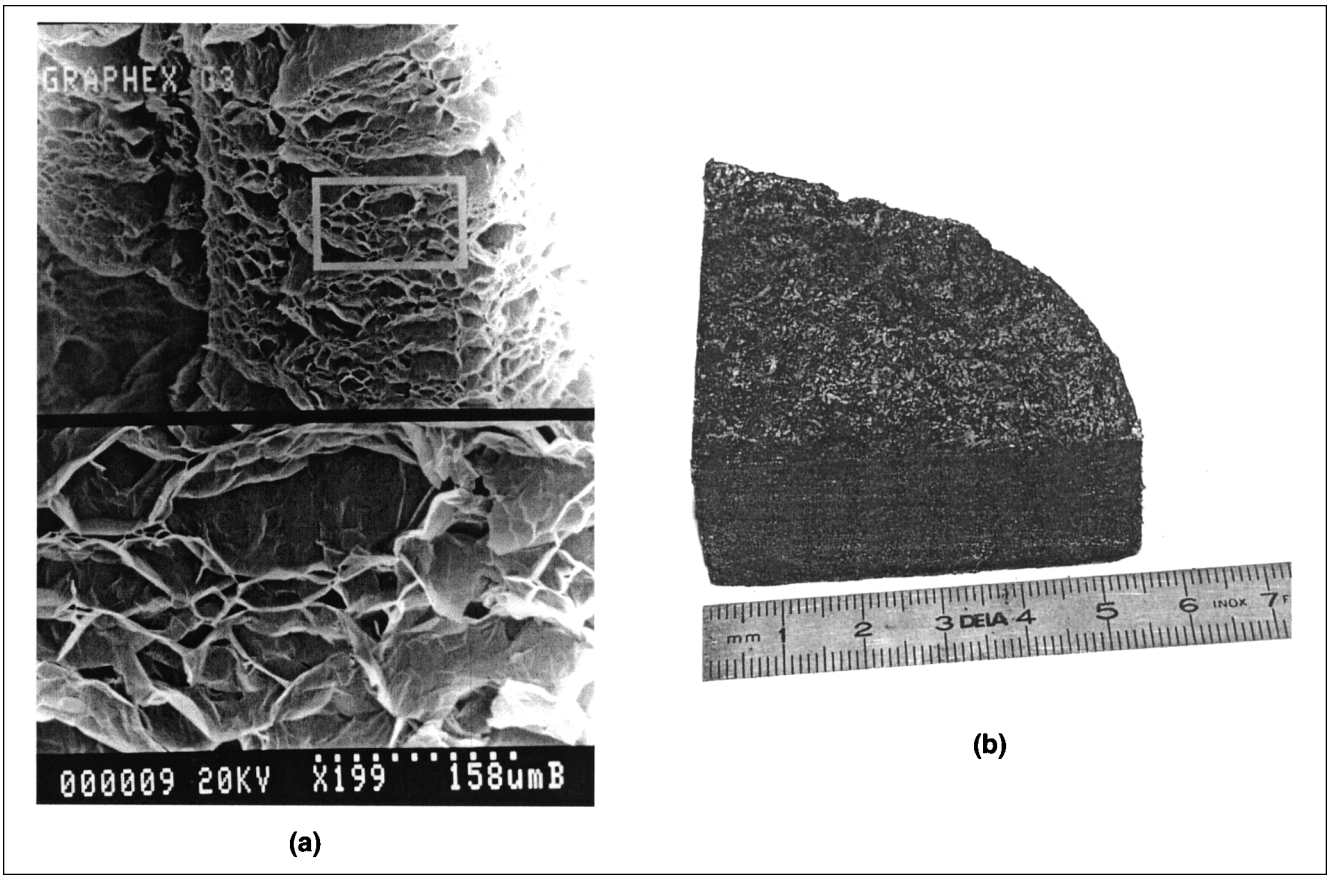


**Figure 2. (a) Scanning electron microscopy of ENG, (b) and photo of ACB.**

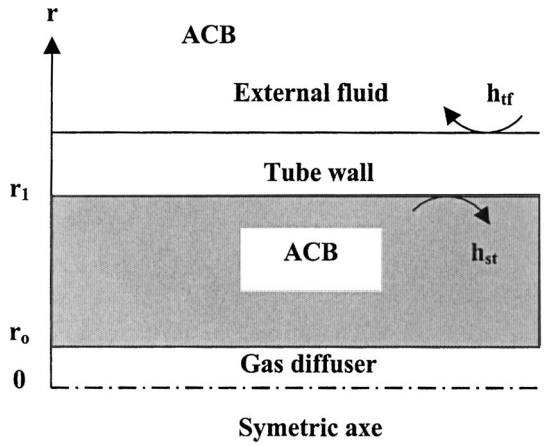


**Figure 3. One-dimensional system.**

and viscosity) are thought to be constant in the range of pressure and temperature (Table 3).

- Fourier's and Darcy's laws determine the heat and mass flow in the composite, respectively.
- The adsorbed gas phase and the solid are locally in equilibrium with the gaseous phase. One assumes the superposition of a local equilibrium (Mota, 1995).
- According previous studies (Mota et al., 1997a; Lamari et al., 2000), natural convection inside the reactor was neglected.

### *Heat and mass balances in the adsorbent composite block*

According to the general assumptions, the mass balance in the ACB is given by:

$$\frac{\partial}{\partial t}\left[\epsilon_o(q)\rho_g + \rho_s q\right] + \nabla\cdot(\rho_g u_g) = 0, \tag{1}$$

where $\epsilon_o$ is the accessible porosity for the gas, and varies with the amount of adsorbed $q$ (Biloé et al., 2001). The gas density, $\rho_g$, and the amount adsorbed, $q$, are related to both the local pressure $P$ and the local temperature $T$ according to the ideal gas equation and the well-known Dubinin-Astakhov (DA) equation (Dubinin and Astakhov, 1971) respectively:

$$\rho_g = \frac{M_g P}{RT}, \tag{2}$$

$$q(P,T) = \rho_a W_o \exp\left[-\left(\frac{A}{\beta E_o}\right)^n\right]. \tag{3}$$

The Polanyi's adsorption potential $A$ (Polanyi and Welke, 1928) is given by

$$A = RT\ln\left(\frac{P_s}{P}\right), \tag{4}$$

where $P_s$ is the saturated vapor pressure. The adsorbed gas density $\rho_a$, and the saturated vapor pressure $P_s$, were calculated according to Dubinin's and Osawa's expressions, respectively (Dubinin, 1975; Osawa et al., 1976). The superficial velocity of the gaseous phase, $u_g$, in the ACB is determined by the Darcy's law (Dullien, 1992):

$$u_g = -\frac{k}{\mu_g}\nabla P. \tag{5}$$

The heat balance in the ACB is given by

$$\frac{\partial}{\partial t}(C_t,T) - \nabla\cdot(\lambda\nabla T) - \rho_s\frac{|\Delta h|}{M_g}\frac{\partial q}{\partial t} = 0, \tag{6}$$

where $C_t$ is the overall volumetric heat capacity:

$$C_t = (\rho C_p)_s + q(\rho C_p)_a, \tag{7}$$

where $(\rho C_p)_s$ and $(\rho C_p)_a$ are the volumetric heat capacity of ACB and the adsorbed gas phase, respectively. Here, the volumetric heat capacity of the gaseous phase is considered negligible. On the other hand, the heat capacity per unit mass of the adsorbed gas phase, $(C_p)_a$, has been taken to be equal to that of the liquid phase (Table 3). The mass balance (Eq. 1) and the heat balance (Eq. 7) are coupled through the dependence of $q$ with respect to $T$ and $P$. The initial conditions are:

$$T(r,t=0) = T_o, \tag{8}$$

$$P(r,t=0) = P_c, \tag{9}$$

where $T_o$ and $P_c$ are the room temperature and the charge pressure (3.5 MPa), respectively. The boundary conditions are expressed as follows:

$$\left.\frac{\partial T}{\partial r}\right|_{r=r_o} = 0, \tag{10}$$

$$-\lambda\left.\frac{\partial T}{\partial r}\right|_{r=r_1} = h_{st}\left(T_t - T|_{r=r_1}\right), \tag{11}$$

and

$$\left.\frac{\partial P}{\partial r}\right|_{r=r_1} = 0, \tag{12}$$

where $T_t$ is the temperature of the tube. At $r = r_o$ (gas diffuser border), a constant discharge flow rate, $v$, was applied according to the procedure of calculation described in detail later.

**Table 3. Physical Properties of Maxsorb, ENG, and Tube**

| | ENG | Maxsorb | Tube | Gas ($CH_4$) |
|---|---|---|---|---|
| $\rho(\mathrm{kg\cdot m^{-3}})$ | 112.5 | 337.5 | 8238 | 9.4 |
| $C_p$ $(\mathrm{J\cdot kg^{-1}\cdot K^{-1}})$ | 840 | 1375 | 468 | 2316 |

### *Heat balance for the tube*

The tube exchanges heat with the ACB and the external fluid through a heat exchange coefficient $h_{st}$ and $h_{tf}$, respectively (Figure 3).

The heat equation for the tube is written as

$$(\rho C_p)_t \frac{\partial T_t}{\partial t} = \frac{h_{st} S_{st}}{V_t}\left(T|_{r=r_1} - T_t\right) + \frac{h_{tf} S_{tf}}{V_t}\left(T_f - T_t\right), \quad (13)$$

where $S_{st}$ and $S_{tf}$ are the different exchange surfaces, and $V_t$ is the volume of the tube wall. The external fluid can be water or air. In both cases, a constant temperature $T_f$ defines the external fluid. The initial conditions for the tube and the external fluid are:

$$T_t = T_f = T_o. \quad (14)$$

## *Model Parameter Values and Resolution Method*

Both the transfer and microporous properties of ACB are listed on Table 2. The obtained values have been measured using the experimental apparatus and procedure developed by CNRS-IMP. In this section, a brief description of the experimental device and procedure is presented. A more detailed description has been given elsewhere (Biloé et al., 2001; Mauran et al., 2001; Olivés and Mauran, 2001).

### *Adsorption isotherm and isosteric heat of adsorption*

The microporous properties of activated carbon in the ACB were determined by $CH_4$ adsorption. Adsorption isotherms were performed using a high-pressure volumetric device (Guillot et al., 1997) under pressure up to 7 MPa and at three temperature levels (253 K, 273 K, and 298 K). The microporous structures derived from Dubinin-Astakhov analysis are listed in Table 2. Due to the fact that ENG is inert with respect to the adsorption of methane, the microporous characteristics of ACB depend only on the microporous properties of adsorbent, that is, Maxsorb. Thus, the DA analysis was applied from the corrected (in mass of ENG) adsorption isotherms. The isosteric heat of adsorption was calculated from the slopes of the experimental curves $\ln(P/P_0)$ vs. $-1/T$, derived from adsorption isotherms. The obtained value was closed to 16 $kJ \cdot mol^{-1}$.

### *Heat- and mass-transfer properties of ACB*

The effective thermal conductivity was determined by the current method of the one-dimensional steady-state heat flow. A small sample of ACB of cubic section (2.5 cm) was placed between two standard bars of known thermal conductivity (aluminum, ceramic, and so on). The heat flow was imposed through both the sample and the standard bars, via two plates at controlled temperature. Thermal conductivity is close to 7.3 $W \cdot m^{-1} \cdot K^{-1}$. The obtained value is about 40 times larger than that of an activated carbon packed bed (Cacciola et al., 1995). The high conductivity results from both the high intrinsic conductivity of graphite and very good contacts between the graphite planes and superactivated carbon powder. A model has been described elsewhere (Olivès and Mauran, 2001) that correlate the thermal conductivity at a different weight ratio of ENG ($w_1$) and according to different apparent densities ($\rho_s$).

The permeability is calculated so that the simulated fields of pressure and discharge flow rate are fitted on those experimental results. The permeability is the only term that is identified in the proposed model. The value obtained is close to $1 \times 10^{-14}$ $m^2$. This value is in relatively good agreement with that given elsewhere on ACBs with various densities and mass weight of ENG (Biloé et al., 2001). Permeability is smaller than that of powdered activated carbon without consolidation ($10^{-10}$–$10^{-12}$ $m^2$). The mass transfer in the ACB is influenced by the geometric flow path as well as by the accessible porosity. In view of the large accessible porosity of ACB, the low permeability value thus results in a significant tortuosity or low input pore diameter (Mauran et al., 2001). Other studies in progress will make it possible to conclude the discussion.

### *Heat transfer exchange coefficients*

According to various heat-exchange conditions at the reactor wall, the wall-heat transfer coefficient $h_{tf}$ takes different values. In both cases, the wall-heat exchange coefficient $h_{tf}$ is connected with a heat-transfer coefficient by forced convection, which is expressed as a function of Prantl and Reynold numbers by a well-known correlation (Incropera and Dewitt, 1996). If the external fluid is water and for a 4-$L \cdot min^{-1}$ constant water flow rate, the value of $h_{tf}$ is close to 700 $W \cdot m^{-2} \cdot K^{-1}$. On the other hand, if the external fluid is air, the heat-transfer coefficient $h_{tf}$ is about 20 $W \cdot m^{-2} \cdot K^{-1}$.

As regards the heat exchange coefficient $h_{st}$, one supposes that the transfer of heat is not limiting, compared with $h_{tf}$. As a matter of fact, the consolidation procedure ensures a very good contact between the ACB and the surface's reactor. The value selected is 2,500 $W \cdot m^{-2} \cdot K^{-1}$.

### *Resolution method*

The set of nonlinear differential equations (Eq. 1 and Eq. 7) with the initial and boundary conditions (Eqs. 8–12 and 14) are solved by the control-volume method (Patankar, 1980) using an implicit scheme. First, supposing a pressure value in the gas diffuser (taken as the second boundary condition for the mass balance), the fields of pressure and temperature are estimated by an iterative procedure of prediction–correction. Knowing the pressure and temperature fields at time $t$, the pressure and temperature fields were successively calculated at time $t + dt$ and compared with those estimated. This procedure was repeated, until a relative convergence criterion of 1% on both the temperature and the pressure was not achieved. It was the first loop of the program. Second, the discharge flow rate was calculated and compared with the one imposed (experimental flow rate). If the both rates were not equal, the pressure in the gas diffuser was reappraised by a dichotomy method on a sequence of interval $[P|_{r=r_o}(t), P_o]$, where $P|_{r=r_o}(t)$ is the estimated gas diffuser pressure at time $t$. The fields of pressure and temperature were recomputed together (by the first loop). Next, the new flow rate

**Table 4. Experimental Conditions**

| No. | $h_{tf}$ ($W \cdot m^{-2} \cdot K^{-1}$) | $v$ ($NL \cdot min^{-1}$) |
|---|---|---|
| Heat external transfer with water (HETW) | 700 | 5 |
| Heat external transfer with air (HETA) | 20 | 10 |

was compared a second time. This procedure was repeated until a second relative convergence criterion of 1% on the discharge flow rate was achieved.

## Results and Discussion

### *Discharge characteristics and model validation*

Experimental and simulated temperature, pressure, and flow-rate profiles, respectively, were determined for both wall-heat exchange coefficients $h_{tf}$ and discharge flow rates $v$. In this section, only two analyses of the discharge of the ANG vessel are presented, according to the two specific experimental conditions (Table 4).

*Temperature Profiles.* Figures 4a and 4b show experimental and simulated temperatures at various radial positions in the reactor, as a function of time for both the HETW and HETA experimental conditions. At first, the ANG cylinder is at room temperature ($T_o$) and charge pressure ($P_c = 3.5$ MPa). At $t = 0$, a constant discharge flow rate is imposed. It leads to imposition of pressure in the gas diffuser. The generated pressure gradient immediately places the ANG vessel in the desorption condition. The reactor cools down due to the heat of desorption, with a minimum temperature near the gas diffuser ($T_1$), of 258 K and 293.5 K for the HETA and HETW experimental conditions, respectively. It corresponds to a 40 K and 5 K temperature drop, respectively. The average temperature drop of the ACB is close to 37 K and 4 K, respectively, under these conditions. At the same time, the wall-temperature drop ($T_t$) is about 35 K and 1.5 K, respectively. Thus, the temperature gradients in the ACB are very small for both experimental conditions. The higher one is close to 5 K for the largest detrimental condition (HETA). These first results indicate the efficiency of ENG. The high value of thermal conductivity ensures enhancement of conductive heat transfer in the ANG vessel, if there is no heat transfer limitation at the reactor wall (that is, for a high value of $h_{tf}$). This allows it to easily supply heat for the desorption step.

For the HETW experimental condition (Figure 4a), the temperature at first decreases slightly in the ACB, after which the reactor follows an isotherm path. This path corresponds to the necessary temperature gradient between the external fluid's temperature (water) and the average temperature of the ACB, to supply the required heat for the desorption step, corresponding to the desired discharge flow rate. This thermal gradient is related for the given surface's reactor to the value of $h_{tf}$.

For the HETA experimental condition (Figure 4b), due to the fact that the wall-heat exchange coefficient $h_{tf}$ is small, the thermal behavior of the ANG vessel is close to adiabatic thermal behavior. The constant decrease in the temperature is directly linked to the endothermic desorption as well as the discharge flow rate.

When the discharge flow rate cannot be ensured any more (at time $t \geq \tau$), the temperature increases. This increase results from the conductive heat transfer in the ACB as well as the heat transfer from the ACB to the environment. Due to the high value of conductivity of the ACB, the time it takes to return to room temperature depends mainly on the value of

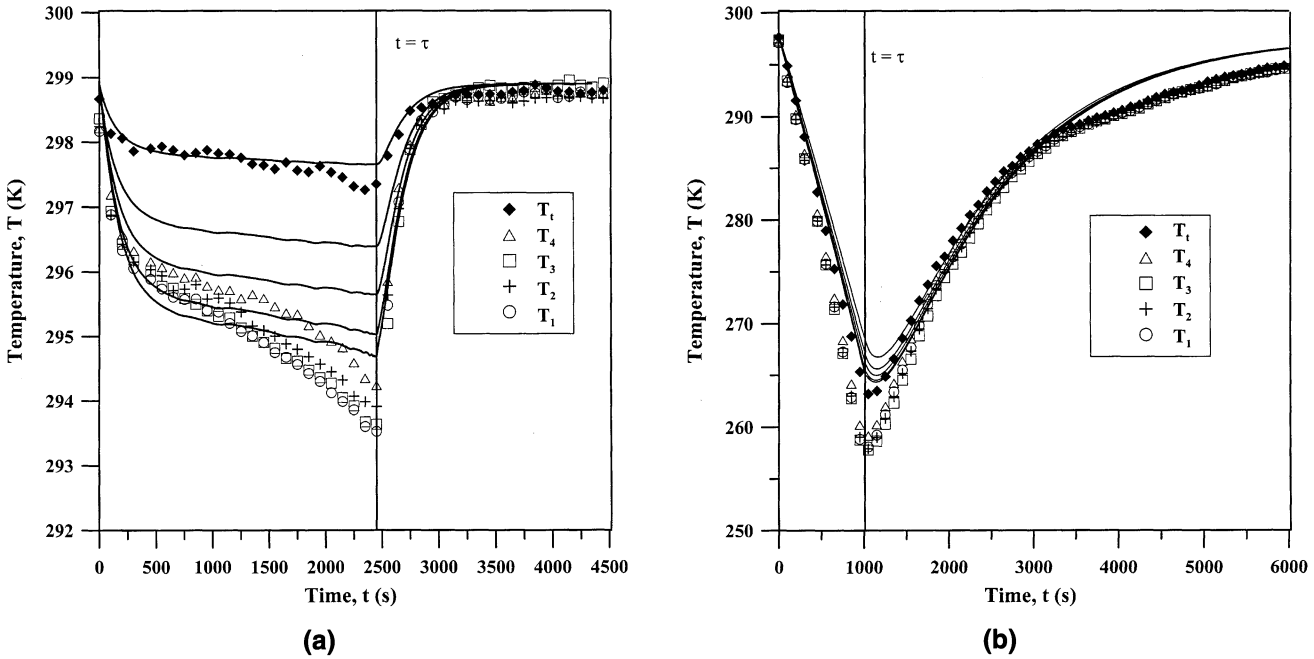


**Figure 4. Experimental (symbols) and simulated (lines) temperatures at different radial positions for (a) HETW and (b) HETA discharge experimental conditions.**

the wall-heat transfer coefficient $h_{tf}$. For example, when the heat transfer to the surroundings is not limited (HETW), the increase in temperature is very fast (15 minutes). On the other hand, from the HETA experimental condition (Figure 4b), one can see that the principal limitation is located at the wall-heat transfer's level, resulting in a longer time before equilibrium ($T_o$) is reached. If it's not critical for the discharge process, it would be the case for the charge step, where the fill's time must be as short as possible.

The delivered methane capacity is close to 94 V/V and 71 V/V for the HETW and HETA experimental conditions, respectively.

*Model Validation.* According to the numerous simplifying assumptions, the model describes very well the dynamic behavior of the ANG vessel. The simulated temperature profiles are in good agreement with the experimental temperature profiles, especially for the experimental condition HETW. The largest discrepancy is close to 1 K.

For the HETA experimental condition, during the discharge step at a constant discharge flow rate ($t < \tau$), the simulated endothermic pick is slightly higher than the experimental one. The difference is close to 7 K. This difference could be explained by the value of the specific heat capacity of the adsorbed gas phase. In addition, during the second regime ($t \geq \tau$), the simulated temperatures are higher than the experimental ones that exceeded 3,500 s. This difference results mainly in gas condensation at the reactor wall, whereas the model assumes both constant temperature and wall-heat exchange coefficient.

Figures 5 and 6 show experimental and simulated pressure profiles in the gas diffuser and discharge flow rate profiles, respectively. The figures show very good agreement between the model and experimental results. This agreement demonstrates the validity of the proposed model.

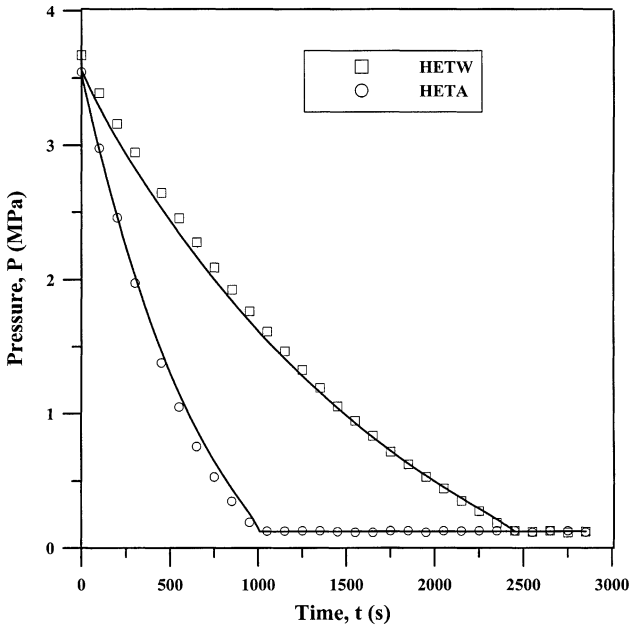


**Figure 5. Experimental (symbols) and simulated (lines) pressure profiles in the gas diffuser for HETW and HETA discharge experimental conditions.**

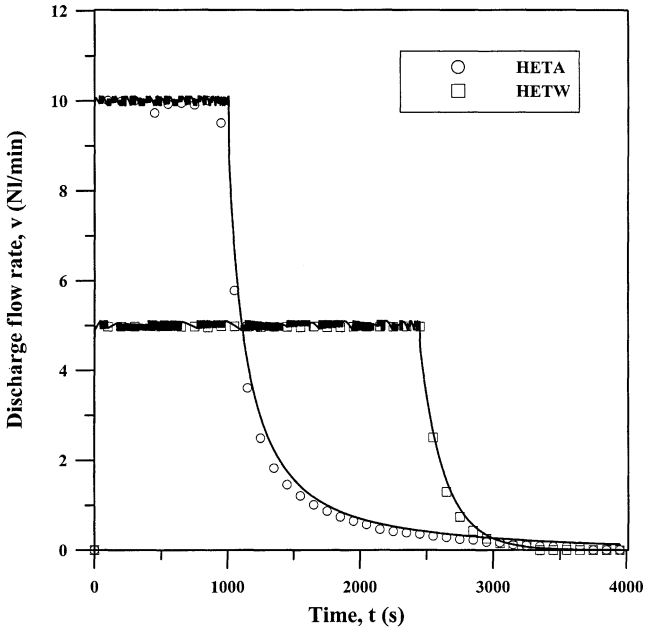


**Figure 6. Experimental (symbols) and simulated (lines) discharge flow-rate profiles for HETW and HETA discharge experimental conditions.**

### *Influence of constant discharge flow rates*

Figure 7 shows the simulated average thermodynamic path of the ACB in the Clausius-Clapeyron diagram for various flow rates, and for the special case of $h_{tf} = 700\ \mathrm{W \cdot m^{-2} \cdot K^{-1}}$. The thermodynamic path depends on the physical properties of the adsorbent (Maxsorb) by way of the isosteres. The straight lines represent the isosteric network, derived from the DA equation (Eq. 3). Each line corresponds to an isostere where the amount of adsorbed gas remains constant. In addition, each line is separated from each other by a constant step equal to 0.012 g $(CH_4) \cdot g^{-1}$ (Maxsorb). The different average paths were calculated from the average volumetric pressure and temperature, respectively, during the desorption step.

For the lowest discharge flow rate, the desorption step is very close to the isothermal condition. At the end of the discharge at constant flow rate ($t = \tau$), the average pressure and temperature, respectively, are close to those at equilibrium ($P_o$, $T_o$).

In general, at the beginning of the discharge step, the pressure gradient immediately places the ANG vessel in the desorption condition. The decrease in the average pressure of the ACB coincides with a decrease in the average temperature. This temperature and pressure drop increases with increasing flow rate. When the rate of discharge cannot be ensured anymore, the limitations by the heat and/or mass transfer becomes effective.

In practice, the desired discharge flow rate cannot be ensured any longer when the pressure in the gas diffuser is equal to 0.1 MPa. Then, the corresponding average pressure and temperature in the ACB, respectively (represented by symbols ○ on Figure 7), allow us to see that this phenomenon (heat and/or mass transfer) is the most limiting one. If the

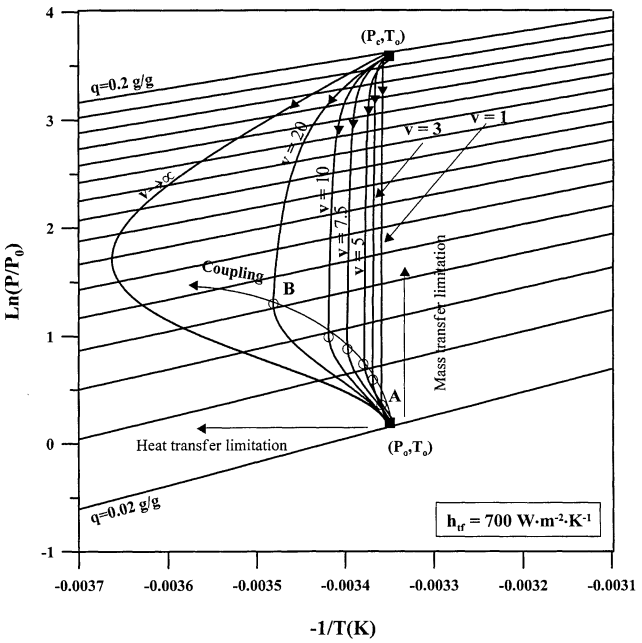


**Figure 7. Influence of discharge flow rates, $v$ ($NL \cdot min^{-1}$), on the average thermodynamic path of ACB in the Clausius-Clapeyron representation.**

The symbols, ○, denote the end of the discharge at constant flow rate ($t = \tau$).

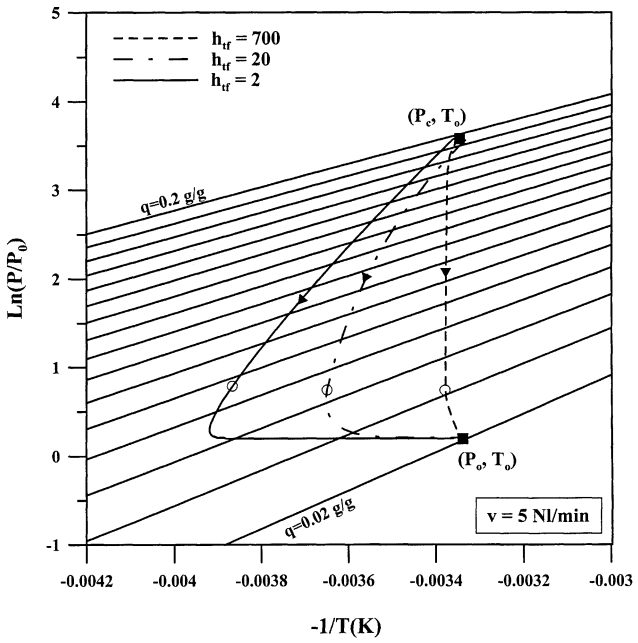


**Figure 8. Influence of wall-heat exchange coefficients, $h_{tf}$ ($W \cdot m^{-2} \cdot K^{-1}$), on the average thermodynamic path of ACB in the Clausius-Clapeyron representation.**

The symbols, ○, denote the end of the discharge at constant flow rate ($t = \tau$).

characteristic point of the system is situated at a pressure far from the depletion pressure ($P_o$), the mass-transfer limitation becomes dominant. Similarly, if the characteristic point of the system is situated at a temperature lower than room temperature ($T_o$), the heat-transfer limitation becomes dominant. This last limitation could result from heat transfer limitation either by conduction in the ACB or by convection outside the reactor wall.

As expected, Figure 7 shows that the limitation of heat and/or mass transfer occurs at an increasingly higher level of pressure and temperature as the discharge flow rate increases. When the discharge flow rate increases from 1 $NL \cdot min^{-1}$ to 20 $NL \cdot min^{-1}$, the average temperature falls from 298 K (A, characteristic point) to 287 K (B, characteristic point), and the average pressure in the ACB goes from 0.12 MPa to 0.35 MPa, respectively.

The heat flux consumed by the endothermic desorption is proportional to the desired discharge flow rate. The increase in the rate of discharge requires increased heat flux in order to reduce the temperature drop.

As shown by Figure 7, for rates less than 10 $NL \cdot min^{-1}$, the thermodynamic paths are similar. After a small temperature drop, the reactor follows an isotherm path. As described previously, the temperature drop corresponds to the temperature gradient, between the water temperature and the average ACB temperature, which is necessary in order to supply the required heat desorption at a given discharge flow rate. This consideration indicates that the rate of heat exchange between the reactor and the surroundings is the rate determining the discharge process. For higher rates, the thermodynamic path is more "rounded," indicating that the heat and mass transfer are coupled.

It's interesting to show the average thermodynamic path of the ACB during a discharge, without controlling the rate of flow ($v \to \infty$), which returns to impose a constant gas pressure in the diffuser close to 0.1 MPa. Figure 7 shows that the reactor cools down to an average temperature level of 273 K in only 53 s. The corresponding average pressure is 0.55 MPa. The complete discharge takes close to 15 min, which shows the good transfer properties of the ACB. The rapid pressure decrease indicates that the mass transfer is not very limiting for this ACB. If it is not realistic to discharge an ANG system under this condition, it would be at the time of the charge step. The good heat and mass transfer of the ACB will be, without all other considerations, very beneficial in terms of charge time, compared with traditional systems not employing ENG. Experimental results to validate this significant aspect are in progress.

### *Influence of wall-heat exchange coefficients*

Figure 8 shows the simulated average thermodynamic path of the ACB in the Clausius-Clapeyron diagram for various wall-heat exchange coefficients. Three wall-heat exchange coefficients were chosen according to three specific experimental conditions: nearly adiabatic desorption, desorption with air, and water, respectively, at a constant discharge flow rate of 5 $NL \cdot min^{-1}$. These different configurations show the importance of the wall-heat transfer limitation.

The temperature drop increases as the wall-heat exchange coefficient decreases. As expected, the higher the wall-heat transfer coefficient the lower the average temperature drop. As described previously, the thermal effects are more important for the lower $h_{tf}$, because the required heat for the desorption is not supplied. For adiabatic desorption, the reactor cools down to 259 K. This corresponds to an average temperature drop of about 30 K. This temperature drop therefore increases the residual amount of gas at depletion pressure, reducing the dynamic delivered methane capacity by 25% compared to isothermal discharge.

However, an interesting aspect must be noted. At the end of the discharge at constant flow rate, the pressure is the same as for all wall-heat exchange configurations. The average pressure in the ACB is close to 0.15 MPa. It is then evident that a small mass-transfer limitation occurs for a 5-NL$\cdot$m$^{-1}$ discharge flow rate. The main limitation is located on the level of heat exchange between wall and the surroundings. Although good heat and mass transfer of ACB have been achieved, it is necessary to maximize the convective heat exchange between the wall and the surroundings. In this article, this has been achieved by axially flowing water around the annular space that surrounds the ANG vessel.

From Figure 8, one can see a very interesting phenomenon. Indeed, in spite of a very significant drop in temperature, the adsorbent is practically desorbed at the end of the discharge at constant flow rate. This is caused by the position of the isosteres in the Clausius-Clapeyron diagram. Thus, a small amount of gas remains at depletion pressure. The activated carbon used is thus ideal for the desorption step, which explains why it is so often used for this process.

### *Impact of ENG on performances of ANG systems*

The performance of ANG systems is usually defined as the methane volume delievered, measured at normal conditions ($P = 0.1$ MPa, $T = 273.15$ K) per adsorbent volume. ANG must have a value close to 150 V/V if it is to be economically competitive with CNG (Parkyns and Quinn, 1996).

Under real working conditions (constant discharge flow rate), the impact of ENG on performances is evaluated by the dynamic efficiency$\eta$. This is defined as follows

$$\eta = \frac{Q_{dd}}{Q_{di}}, \tag{15}$$

where $Q_{dd}$ and $Q_{di}$ are the delivered gas volume per adsorbent volume under dynamic conditions and isothermal condition, respectively.

The delivered methane volume per adsorbent volume under isothermal conditions is close to 100 V/V. This value is more likely due to the high micropore volume of Maxsorb than to its density in the ACB (337.5 kg$\cdot$m$^{-3}$).

Figure 9 shows experimental and simulated values of dynamic efficiency vs. the discharge flow rate with respect to the two wall-heat exchange conditions. Good accuracy can be seen between experimental and simulated results. The largest discrepancy is not more than 5%, again showing the validity of the proposed model.

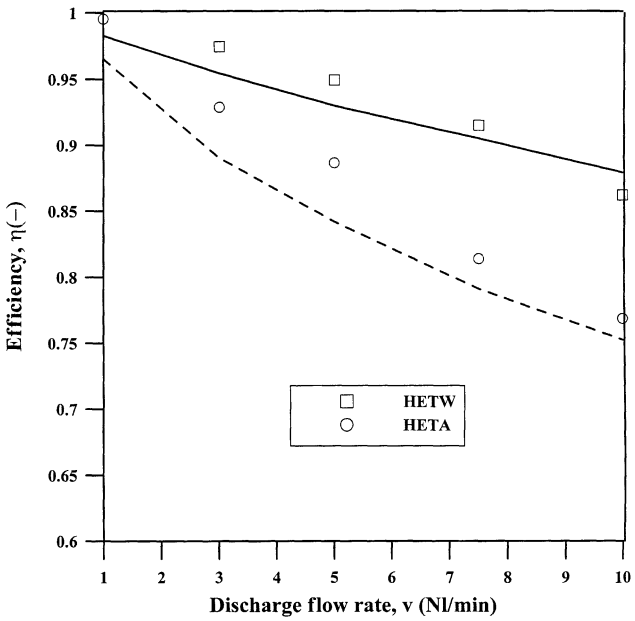


**Figure 9. Dynamic efficiencies vs. various constant discharges flow rates.**

The symbols and the curves denote the experimental results and model, respectively.

For discharge flow rates less than 5 NL$\cdot$min$^{-1}$ and the prevailing wall-heat exchange conditions, except adiabatic desorption, the dynamic efficiency is greater than 90%. So the delivered methane capacity was situated between 90 and 100 V/V.

Beyond 5 NL$\cdot$min$^{-1}$, the dynamic efficiency decreases because the required heat to desorption is not enough. This phenomenon results more in wall-heat exchange limitations than in heat- and mass-transfer properties of the ACB. As described previously, the transfer properties of the monolith are less limiting, ensuring both very weak thermal gradients in the reactor and rapid discharge step.

## Conclusion

ANG technology is an attractive alternative for reducing both the high pressures and cryogenic temperatures required for current gas storage (CNG, LNG). Most of the scientific research has been focused on the development of highly microporous adsorbents. A performance level of 150 V/V has been achieved already, but from theoretical calculations that derived from adsorption isotherms. Nevertheless, thermal effects dramatically reduce the delivered methane capacity. Current adsorbents are not adapted because of their very low conductivity ($\lambda = 0.2$ W$\cdot$m$^{-1}\cdot$K$^{-1}$). One of the solutions was to use an inert binder as the conductive medium.

In this article, the thermal behavior of ANG vessel discharge with a new adsorbent composite block has been investigated. The ACB consisted of an inert graphite binder (expanded natural graphite) and Maxsorb, the well-known activated carbon. The reactive mixture obtained has very interesting transfer and adsorption properties.

The first objective was to evaluate the practicable use of this ACB under various dynamic and realistic conditions. Therefore, an experimental test rig was set up. In addition, a general model was formulated, based on previous research. This model couples the heat and mass transfer of the ACB. Simulated results were validated by several experimental conditions, including various constant discharge flow rates and wall-heat exchange conditions. Simulated and experimental results showed the efficiency of the proposed ACB during the desorption step. This efficiency leads successfully to a delivered methane capacity close to 100 V/V under various practical dynamic conditions. For a cruising radius of 300 km, a natural-gas vehicle traveling at normal speed needs 52 L of reactor (for 100 delivered gas volume per reactor volume). Reduced to the tested 2-L experimental reactor, the required discharge flow rate is closed to 1 $NL \cdot min^{-1}$. For this rate and the current wall-heat exchange conditions, the ANG vessel works according to isothermal conditions (Figure 9).

The next important step will be to optimize the ACB for both the charge and discharge steps. The objective will be to minimize the charge time and to maximize the delivered methane capacity under dynamic conditions while increasing the adsorbent density in the ACB. This objective bypasses by the acquisition of the transfer properties of many ACBs with various implementations. Further studies are already in progress.

## Notation

$E_o$ = characteristic energy of adsorption, $J \cdot mol^{-1}$
$k$ = permeability, $m^2$
$n$ = DA exponent
$P$ = pressure, Pa
$r$ = radius, m
$R$ = perfect gas constant, $J \cdot mol^{-1} \cdot K^{-1}$
$T$ = temperature, K
$W_o$ = total microporous volume, $cm^3 \cdot g^{-1}$

### *Greek letters*

$\beta$ = affinity coefficient
$\Delta h$ = isosteric heat of adsorption, $J \cdot mol^{-1}$
$\lambda$ = conductivity, $W \cdot m^{-1} \cdot K^{-1}$
$\mu_g$ = gas viscosity, $Pa \cdot s$

### *Subscripts*

$a$ = adsorbed
$dd$ = delivered under dynamic conditions
$di$ = delivered under isothermal conditions
$f$ = fluid
$g$ = gas
$s$ = solid
$st$ = solid-tube
$t$ = tube
$tf$ = fluid-tube

## Literature Cited


Alcañiz-Monge, J., M. A. De La Casa-Lillo, D. Cazorla-Amóros, and A. Linares-Solano, "Methane Storage in Activated Carbon Fibres," *Carbon*, **35**, 291 (1997).

Baker, F. S., "Highly Microporous Carbon," U.S. Patent No. 5,710,092 (1998).

Biloé, S., V. Goetz, and S. Mauran, "Characterization of Adsorbent Composite Blocks for Methane Storage," *Carbon*, **39**, 1653 (2001).

Bose, T. K., R. Chahine, and J. M. St-Arnaud, "High-Density Adsorbent and Method of Producing Same," U.S. Patent No. 4,999,330 (1991).

Cacciola, G., G. Restuccia, and L. Mercadante, "Composites of Activated Carbon for Refrigeration Adsorption Machines," *Carbon*, **33**, 1205 (1995).

Carrott, P. J. M., M. M. L. Ribeiro, I. P. P. Cansado, and J. M. V. Nabais, "Reference Data for the Adsorption of Benzene on Carbon Materials," *Carbon*, **38**, 465 (2000).

Chang, K. J., and O. Talu, "Behaviour and Performance of Adsorptive Natural Gas Storage Cylinders During Discharge," *Appl. Therm. Eng.*, **16**, 359 (1996).

Cook, T. L., and D. B. Horne, "Low Pressure Adsorbed Natural Gas Vehicle Demonstration," *Proc. World Gas Conf.*, Copenhagen, Denmark, **31** (1997).

De Chauveron, S., "Le Gaz Naturel Vehicule," *Rev. Inst. Fr. Pet.*, **51**, 729 (1996).

Dubinin, M. M., *Progress Surface and Membrane Science*, Vol. 9, Chap. 1, D. A. Cadenhead, eds., New York (1975).

Dubinin, M. M., and V. A. Astakhov, "Description of Adsorption Equilibrium of Vapours on Zeolites over Wide Ranges of Temperature and Pressure," *Adv. Chem. Ser.*, **102**, 69 (1971).

Dullien, F. A. L., *Porous Media: Fluid Transport and Pore Structure*, 2nd ed., Academic Press, San Diego (1992).

Ferriére, A., S. Biloé, and S. Mauran, "A Solar Process for the Exfoliation of Graphite Intercalated Compounds," *Proc. Inst. Symp. on Solar Thermal Concentrating Tech.*, H. Kreetz, K. Lovegrove, and W. Meike, eds., Sydney, Australia, p. 277 (2000).

Guillot, A., S. Follin, and L. Poujardieu, "Adsorption Studies of Carbon Dioxide on KF1500, X2MH6/8 and PX21 by Means of a High Pressure Volumetric Device," *Characterization of Porous Solids IV*, B. McEnaney, T. Nays, J. Rouquérol, F. Rodriquez-Reinoso, K. S. W. Sing, K. K. Unger, eds., The Royal Society of Chemistry, London, p. 573 (1997).

Incropera, F. P., and D. P. Dewitt, *Fundamentals of Heat and Mass Transfer*, 4th ed., Wiley, New York (1996).

Jasionowski, W. J., A. J. Tiller, J. A. Fata, J. M. Arnold, S. W. Gauthier, and Y. A. Shiraki, "Charge-Discharge Characteristics of High-Capacity Methane Adsorption Storage Systems," *Proc. Int. Gas Res. Conf.*, Tokyo, Japan, p. 1192 (1989).

Kaneko, K., and K. Murata, "An Analytical Method of Microporous Filling of a Supercritical Gas," *Adsorption*, **3**, 197 (1997).

Lamari, M., A. Aoufi, and P. Malbrunot, "Thermal Effects in Dynamic Storage of Hydrogen by Adsorption," *AIChE J.*, **46**, 632 (2000).

Lepinasse, E., V. Goetz, and G. Crozat, "Modelling and Experimental Investigation of a New Type of Thermochemical Transformer Based on the Coupling of two Solid-Gas Reactions," *Chem. Eng. Proc.*, **33**, 125 (1994).

Loughlin, K. F., M. M. Hassan, A. I. Fatehi, and M. Zahur, "Rate and Equilibrium Sorption Parameters for Nitrogen and Methane on Carbon Molecular Sieve," *Gas Sep. Purif.*, **7**, 264 (1993).

MacDonald, J. A. F., and D. F. Quinn, "Adsorbents for Methane Storage Made by Phosphoric Acid Activation of Peach Pits," *Carbon*, **34**, 1103 (1996).

MacDonald, J. A. F., and D. F. Quinn, "Carbon Adsorbents for Natural Gas Storage," *Fuel*, **77**, 61 (1998).

Manzi, S., D. Valladares, J. Marchese, and G. Zgrablich, "Characterization of Maxsorb Activated Carbons and Their Evaluation for Gas Storage," *Adsorp. Sci. Technol.*, **15**, 301 (1997).

Mauran, S., L. Rigaud, and O. Coudevylle, "Application of the Carman-Kozeny Correlation to a High-Porosity and Anisotropic Consolidated Medium: The Compressed Expanded Natural Graphite," *Transp. in Porous Media*, **43**, 355 (2001).

Mauran, S., M. Lebrun, P. Prades, M. Moreau, B. Spinner, and C. Drapier, "Active Composite and Its Use as Reactive Medium," U.S. Patent No. 5,283,219 (1994).

Mauran, S., P. Prades, and F. L'Haridon, "Heat and Mass Transfer in Consolidated Reacting Beds for Thermochemical Systems," *Heat Recovery Syst. CHP*, **13**, 315 (1993).

Mota, J. P. B., "Modélisation des Transferts Couplés en Milieux Poreux," PhD Thesis, Institut National Polytechnique de Lorraine, Nancy, France (1995).
Mota, J. P. B., "Impact of Gas Composition on Natural Gas Storage by Adsorption," *AIChE J.*, **45**, 986 (1999).
Mota, J. P. B., A. E. Rodrigues, E. Saatdjian, and D. Tondeur, "Dynamics of Natural Gas Adsorption Storage Systems Employing Activated Carbon," *Carbon*, **35**, 1259 (1997a).
Mota, J. P. B., A. E. Rodrigues, E. Saatdjian, and D. Tondeur, "Charge Dynamics of a Methane Adsorption Storage System: Intraparticle Diffusional Effects," *Adsorption*, **3**, 117 (1997b).
Mota, J. P. B., E. Saatdjian, D. Tondeur, and A. E. Rodrigues, "A Simulation Model of a High-Capacity Methane Adsorptive Storage System," *Adsorption*, **1**, 17 (1995).
Olivès, R., and S. Mauran, "An Highly Conductive Porous Medium for Solid-Gas Reactions. Effect of the Dispersed Phase on the Thermal Tortuosity," *Transp. Porous Media*, **53**, 377 (2001).
Osawa, S., S. Kusumi, and Y. Ogino, "Physical Adsorption of Gases at High Pressure. An Improvement of Dubinin-Astakhov Equation," *J. Colloid Interface Sci.*, **56**, 83 (1976).
Otowa, T., R. Tanibata, and M. Itoh, "Production and Adsorption Characteristics of MAXSORB: High-Surface-Area Active Carbon," *Gas Sep. Purif.*, **7**, 241 (1993).
Parkyns, N. D., and D. F. Quinn, "Natural Gas Adsorbed on Carbon," *Porosity in Carbons*, J. W. Patrick, ed., Chap. 11, Arnold, London, p. 291 (1995).
Patankar, S. V., *Numerical Heat Transfer and Fluid Flow*, McGraw-Hill, New York (1980).
Polanyi, M., and K. Welke, "Adsorption, Adsorptionswarme und Bindungscharakter von Schwefeldioxyd an Khole bei Geringen Belegungen," *Z. Phys. Chem*., **132**, 371 (1928).
Py, X., R., Olivès and S. Mauran, "Paraffin/Porous-Graphite Matrix Composite as a High and Constant Power Thermal Storage Material," *Int. J. Heat Mass Transfer*, **44**, 2727 (2001).
Quirke, N., and S. R. R. Tennison, "The Interpretation of Pore Size Distributions of Microporous Carbons," *Carbon*, **34**, 1281 (1996).
Rychlicki, G., and A. P. Terzyk, "Energetics of Methane Adsorption on Microporous Activated Carbons," *J. Therm. Anal.*, **45**, 1183 (1995).
Salem, M. M. K., P. Braeuer, M. V. Szombathely, M. Heuchel, and K. Quitzsh, "Thermodynamics of High-Pressure Adsorption of Argon, Nitrogen, and Methane on Microporous Adsorbents," *Langmuir*, **14**, 3376 (1998).
Schwarz, J. A., K. Putyera, T. J. Bandosz, J. Jagiello, and K. A. G. Amankwah, "Composite Microporous Carbons for Fuel Gas Storage," U.S. Patent No. 5,837,741 (1998).
Talu, O., "An Overview of Adsorptive Storage of Natural Gas," *Proc. Int. Conf. on Fundamentals of Adsorption*, M. Suzuki, ed., Kyoto, Japan, p. 655 (1992).
Toyoda, M., and M. Inagaki, "Heavy Oil Sorption Using Exfoliated Graphite. New Application of Exfoliated Graphite to Protect Heavy Oil Pollution," *Carbon*, **38**, 199 (2000).
Union Carbide Trademark, "Flexible Graphite Material of Expanded Particles Compressed Together," U.S. Patent No. 3,404,061 (1968).
Wegrzyn, J., and M. Gurevich, "Adsorbent Storage of Natural Gas," *Appl. Energy*, **55**, 71 (1996).
Yoshida, A., and Y. Hishiyama, "Exfoliated Graphite from Various Intercalation Compounds," *Carbon*, **29**, 1227 (1991).
Zhou, Z., "Thermal Analysis of Slow Discharge from a Pressurized Natural Gas Storage Tank," *Appl. Therm. Eng.*, **17**, 1099 (1997).
*Manuscript received Dec. 15, 2000.*